Heliyon 9 (2023) e15984

Contents lists available at ScienceDirect

Heliyon

journal homepage: www.cell.com/heliyon

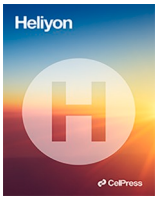

Research article

Epicardial and thoracic subcutaneous fat texture analysis in patients undergoing cardiac CT

Manfredi Agnese [a], Patrizia Toia [a], Giulia Sollami [a], Carmelo Militello [b], Leonardo Rundo [c], Salvatore Vitabile [a], Erica Maffei [d], Francesco Agnello [a], Cesare Gagliardo [a], Emanuele Grassedonio [a], Massimo Galia [a], Filippo Cademartiri [d], Massimo Midiri [a], Ludovico La Grutta [e,*]

[a] *Department of Biomedicine, Neurosciences and Advanced Diagnostics - BIND, University of Palermo, Via del Vespro 127, 90100, Palermo, Italy*
[b] *Institute for High-Performance Computing and Networking, National Research Council (ICAR-CNR), Palermo, Italy*
[c] *Department of Information and Electrical Engineering and Applied Mathematics (DIEM), University of Salerno, Salerno, Italy*
[d] *Department of Radiology, Fondazione Monasterio, Pisa, Italy*
[e] *Department of Health Promotion, Mother and Child Care, Internal Medicine and Medical Specialties - ProMISE, University of Palermo, Palermo, Italy*

A R T I C L E I N F O

Keywords:
Epicardial fat
Texture analysis
Cardiac computed tomography
Cardiovascular risk

A B S T R A C T

Introduction: The aim of our study was to evaluate the feasibility of texture analysis of epicardial fat (EF) and thoracic subcutaneous fat (TSF) in patients undergoing cardiac CT (CCT).
Materials and methods: We compared a consecutive population of 30 patients with BMI $\leq$25 kg/m^2 (Group A, 60.6 $\pm$ 13.7 years) with a control population of 30 patients with BMI >25 kg/m^2 (Group B, 63.3 $\pm$ 11 years). A dedicated computer application for quantification of EF and a texture analysis application for the study of EF and TSF were employed.
Results: The volume of EF was higher in group B (mean 116.1 cm^3 vs. 86.3 cm^3, p = 0.014), despite no differences were found neither in terms of mean density (−69.5 $\pm$ 5 HU vs. −68 $\pm$ 5 HU, p = 0.28), nor in terms of quartiles distribution (Q1, p = 0.83; Q2, p = 0.22, Q3, p = 0.83, Q4, p = 0.34). The discriminating parameters of the histogram class were mean (p = 0.02), 0,1st (p = 0.001), 10_{th} (p = 0.002), and 50_{th} percentiles (p = 0.02). DifVarnc was the discriminating parameter of the co-occurrence matrix class (p = 0.007).
The TSF thickness was 15 $\pm$ 6 mm in group A and 19.5 $\pm$ 5 mm in group B (p = 0.003). The TSF had a mean density of −97 $\pm$ 19 HU in group A and −95.8 $\pm$ 19 HU in group B (p = 0.75). The discriminating parameters of texture analysis were 10_{th} (p = 0.03), 50_{th} (p = 0.01), 90_{th} percentiles (p = 0.04), S(0,1)SumAverg (p = 0.02), S(1,-1)SumOfSqs (p = 0.02), S(3,0)Contrast (p = 0.03), S(3,0)SumAverg (p = 0.02), S(4,0)SumAverg (p = 0.04), Horzl_RLNonUni (p = 0.02), and Vertl_LngREmph (p = 0.0005).
Conclusions: Texture analysis provides distinctive radiomic parameters of EF and TSF. EF and TSF had different radiomic features as the BMI varies.

* Corresponding author. Department of Health Promotion, Mother and Child Care, Internal Medicine and Medical Specialties - ProMISE, University of Palermo, Via Del Vespro 127 90100 Palermo, Italy.
E-mail address: ludovico.lagrutta@unipa.it (L. La Grutta).

https://doi.org/10.1016/j.heliyon.2023.e15984
Received 9 January 2023; Received in revised form 9 April 2023; Accepted 28 April 2023
Available online 5 May 2023

1. Introduction

Nomenclature

EF	epicardial fat
TSF	thoracic subcutaneous fat
CCT	cardiac computer tomography
BMI	body mass index
ROI	region of interest

Epicardial fat (EF) is the adipose tissue between the epicardium and the myocardium. The EF constitutes the subepicardial layer, where the coronary vessels run [1]. It is more represented in men than in women [2] increasing with age [3]. EF is more represented along the right acute edge of the heart, compared to the left acute edge, on the anterior surface, and in the cardiac apex. Furthermore, EF encloses the coronary arteries in the atrioventricular groove and along the anterior and posterior interventricular grooves [2,3]. EF performs relevant physiological functions: mechanical support, preventing the torsion of the coronary arteries during the cardiac contraction; homeostasis of fatty acid in the coronary microcirculation; local energy source for the heart muscle, especially during exercise; thermogenic role, protecting the myocardium from hypothermia.

An increase of EF is considered a novel cardiovascular risk factor of coronary artery disease (CAD), similarly to the visceral fat [4–6]. The increase of EF thickness is associated with an increase in visceral fat [7] and diabetes [8]. Furthermore, EF produces interleukin-6 (IL-6), tumor necrosis factor α (TNF α), chemokines, and adipokines with inflammatory activity [9].

EF can be assessed in-vivo with radiological techniques including echocardiography, MRI or CT scans [10]. CT can provide accurate quantification of EF with computer assisted tools based on HU attenuation [11], but still no radiomic texture analysis was applied in this field [8].

In our study, we assessed the characteristics of EF analysed with a dedicated computer application and a texture analysis radiomic application in a population of patients who underwent Cardiac CT (CCT). Secondly, we evaluated the characteristics and the radiomic features of TSF.

2. Materials and Methods

2.1. Study population

We analysed a population of 60 patients who underwent CCT for suspected CAD between January 2020 and March 2020 at our university medical institution. We excluded from the present analysis patients with history of known CAD. We compared a consecutive

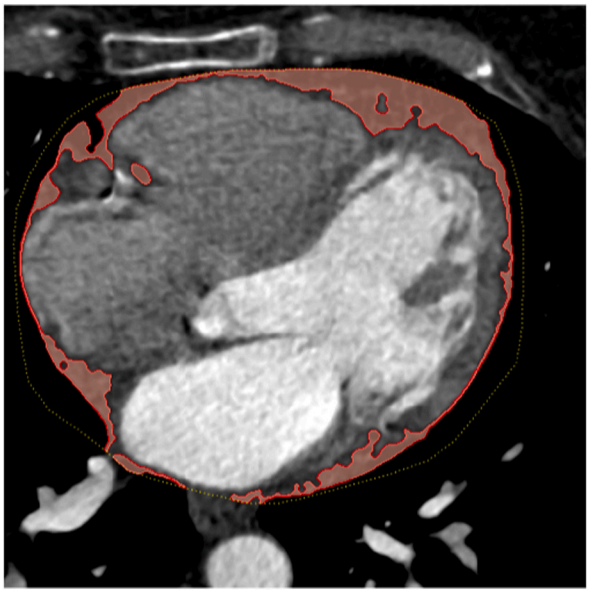

Fig. 1. Quantification of EF with semiautomatic dedicated software. A plane obtained at a four-chamber cardiac view was selected to detect EF displayed in red colour. (For interpretation of the references to colour in this figure legend, the reader is referred to the Web version of this article.)

population of 30 patients with BMI $\leq$25 kg/m^2 (defined as Group A) with a consecutive population of 30 patients with BMI >25 kg/m^2 (defined as Group B). Cardiovascular risk factors (family history, smoking, diabetes, hypertension and hypercholesterolemia) were recorded.

Institutional review board approval was not required since retrospective data of CCT obtained for clinical purposes were employed. All patients signed written informed consent for the administration of ionizing radiation from CCT.

2.2. Epicardial fat and thoracic subcutaneous analysis

All patients were scanned with a 128 slice CT scanner (Definition AS, Siemens Healthcare, Forchheim, Germany). Coronary artery calcium score was performed with the following parameters: 3 mm thickness, 1.5 reconstruction interval, prospective triggering. CCT angiography protocol employed the following parameters: detectors/collimation 64 $\times$ 2/0,6 mm with z-flying focal spot technique; gantry rotation time 300 ms (effective temporal resolution 150 ms); 100–120 kV according to patients body habitus; 160 mAs per rotation; pitch 0,22; table feed 28,2 mm/s; ECG-based tube current modulation. Patients with a heart rate >65 bpm (without known contraindications to b-blockers) were given a dose of 20–40 mg of propranolol orally 1 h prior to the scan or a 5 mg i.v. dose of atenolol prior to the examinations to lower the heart rate. A bolus of 80 ml of nonionic iodinated contrast material (Iomeprol 400 mI/ml, Iomeron, Bracco, Italy) at an injection rate of 5 ml/s, followed by 40 ml of saline solution at the same injection rate, was administered through the antecubital vein of the right arm using a dual-head automatic injector (Stellant, MedRAD, Pittsburgh, PA, USA). Reconstruction parameters of CCT angiography were as follows: effective slice thickness 0,75 mm; increment 0,4 mm; standard smooth convolution filters.

We analysed EF both in terms of volume (cm^3) and mean density (HU) using a dedicated computer application recently developed

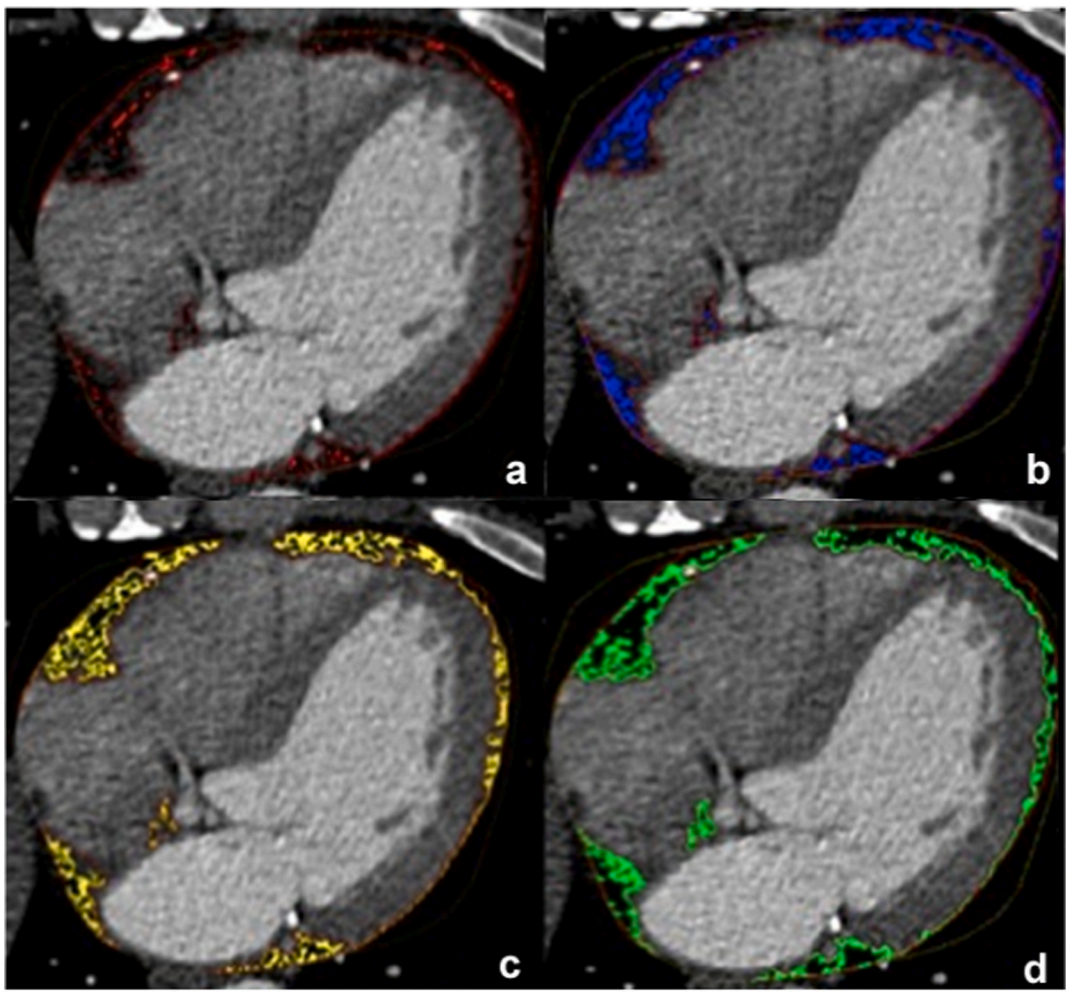

Fig. 2. Maps comparing quartiles density distribution: Q1 (−175 HU, −136 HU), red (a); Q2 (−135 HU, −96 HU), blue (b); Q3 (−95 HU, −56 HU), yellow (c); Q4 (−55 HU, −15 HU), green (d). (For interpretation of the references to colour in this figure legend, the reader is referred to the Web version of this article.)

at our department (Fig. 1), which allows the segmentation and the quantification of the volume, and quartile density distribution (Fig. 2, a-d) [11]. The Agatston coronary calcium score was calculated in both groups [12]. The thoracic subcutaneous fat (TSF) was analysed in each patient. The TSF thickness was measured in terms of mm at the level of carina. The mean attenuation was measured in terms of HU in a region of interest (ROI) of 8 mm^2.

2.3. Radiomics texture analysis

A plane obtained at a four-chamber cardiac view was selected in each patient and each CCT image dataset to detect EF in three representative anatomical landmarks (right atrio-ventricular, anterior interventricular, and left atrioventricular grooves). The images were downloaded from our Picture Archiving and Communication System directly in the bitmap format. Texture analysis was carried out using a free available software (MaZda 4.6, Institute of Electronics, Technical University of Lodz, Lodz, Poland) [13], placing three ROIs in each of the three anatomical landmarks. All ROIs were drawn of identical size with 16 pixels (equivalent to 8 mm^2): the first ROI was placed in the right atrio-ventricular groove (adjacent to the right coronary artery, displayed with a red colour); the second, in the anterior interventricular groove (adjacent to the left anterior descending artery, displayed with a green colour); the third, in the left atrioventricular groove (adjacent to the circumflex branch, displayed with a dark blue colour). We also placed a ROI of identical size in the TSF of each patient (displayed in light blue colour) (Fig. 3a).

The texture analysis software calculated a series of descriptors (n = 294), called radiomic features, for each ROI. Histograms were drawn to represent the intensity values of pixels within the ROIs. The pixel intensity range (Min-Max Brightness) was 0–255 in our study (Fig. 3b).

2.4. Statistical analysis

Continuous variables are expressed as mean ± standard deviation (SD) and categorical variables as percentage. Comparisons between variables were performed with Students *t*-test or ANOVA test for continuous variables and chi-square test for categorical variables. Statistical analysis was performed with SPSS (version 12.0, SPSS Inc., Chicago, IL, United States). Statistical significance was

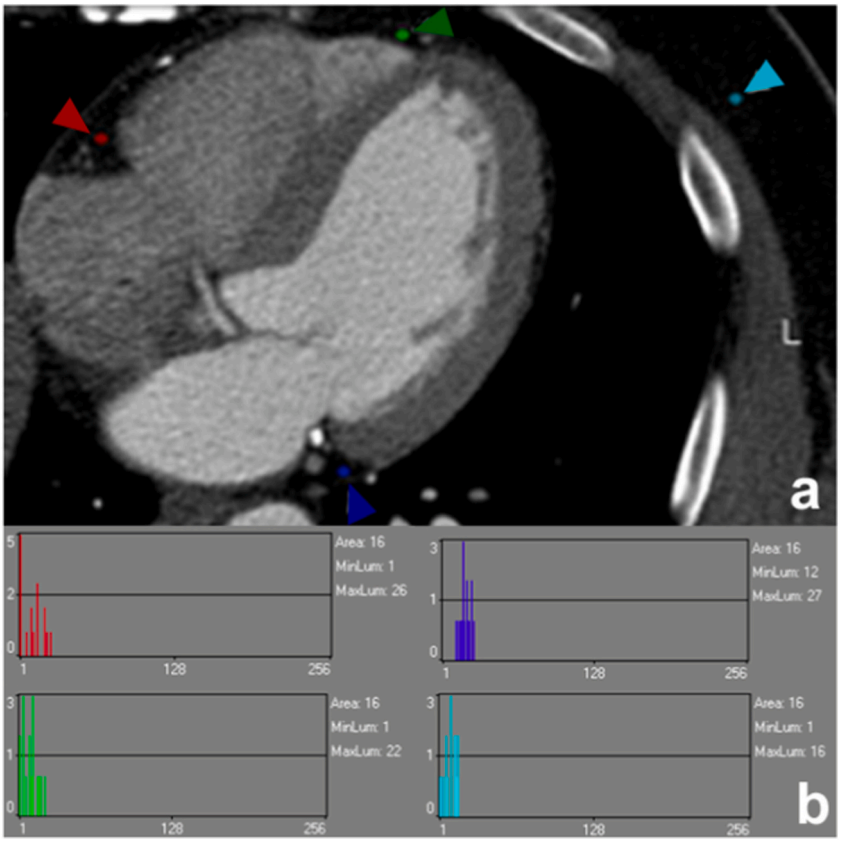

Fig. 3. Radiomic analysis: ROIs in the right atrioventricular groove (red), in the anterior interventricular groove (green), in the left atrioventricular groove (dark blue), and in the thoracic subcutaneous fat (light blue) (a). Histograms representing the intensity values of pixels within the four ROIs: each histogram has the same colour of the relative ROI (b). (For interpretation of the references to colour in this figure legend, the reader is referred to the Web version of this article.)

set at a p value < 0.05.

3. Results

The group A had a BMI $\leq$25 kg/m^2 (mean 22.78 $\pm$ 1.60 kg/m^2, mean age 60.6 $\pm$ 13.7 years, men n = 20), the group B had a BMI >25 kg/m^2 (mean 28.6 $\pm$ 2.89 kg/m^2, mean age 63.3 $\pm$ 11 years, men n = 20). No significant differences were found between patients' characteristics (Table 1).

The average volume of EF was 86.3 $\pm$ 41.8 cm^3 in the group A and 116.1 $\pm$ 49.58 cm^3 in the group B (p = 0.01). The average attenuation of EF was -68 ± 5.46 HU in group A and -69.5 ± 4.9 HU in group B (p = 0.28). No differences were found in terms of quartiles distribution (Q1, p = 0.83; Q2, p = 0.22, Q3, p = 0.83, Q4, p = 0.34). The Agatston coronary calcium score was 97 $\pm$ 167 in the group A and 468 $\pm$ 1410 in the group B (p = 0.15). The TSF had a mean density of -97.3 ± 19.1 HU in group A and -95.8 ± 19 HU in group B (p = 0.75); the thickness of TSF was 15 $\pm$ 6.2 mm in group A and 19.5 $\pm$ 5.3 mm in group B (p = 0.003). The results are summarized in Table 2.

Texture analysis of EF provided five radiomic features with statistically significant differences between the two populations. The discriminating parameters for the histogram class were mean (p = 0.02), 0,1st (p = 0.001), 10_{th} (p = 0.002) and 50_{th} percentiles (p = 0.02). DifVarnc (difference of variance) was the discriminating parameter (p = 0.007) for the co-occurrence matrix class. All the other radiomic features showed no statistically significant differences between the two populations, i.e. skewness (p = 0.25); kurtosis (p = 0.96); S (1, -1) Entropy (p = 0.09); S (1, -1) Contrast (p = 0.058). Results are summarized in Table 3 and plotted in Fig. 4.

In the group A, the discriminating parameters of texture between the ROIs were S(2,0)Correlat (p = 0.04), S(3,0)Correlat (p = 0.04), and S(4,0)Correlat (p = 0.03) in the right atrio-ventricular groove. In the group B the discriminating parameter of texture between the ROIs was S(0,3)Correlat (p = 0.04) in the anterior interventricular groove. Results are summarized in Table 4. We also checked for differences between radiomic features comparing red, green and blue ROIs of group A with corresponding red, green and blue ROIs of group B and we didn't find any significant difference in any of the 294 features.

Texture analysis of TSF provided ten radiomic features with significant differences between the two populations. The discriminating parameters for the histogram class were 10_{th} (p = 0.03), 50_{th} (p = 0.01), and 90_{th} percentiles (p = 0.04), with higher average values in the group A. The discriminating parameters for the co-occurrence matrix class were S(0,1)SumAverg (p = 0.02), S(1,-1) SumOfSqs (p = 0.02), S(3,0)Contrast (p = 0.03), S(3,0)SumAverg (p = 0.02), and S(4,0)SumAverg (p = 0.04), with higher average values in the group A. The discriminating parameters for the run-length matrix were Horzl_RLNonUni (p = 0.02), with higher average value in the group A, and Vertl_LngREmph (p = 0.0005), with higher average value in the group B. Results are summarized in Table 5 and plotted in Fig. 5.

4. Discussion

The EF recently aroused great interest, because it produces substances, such as adipokines and cytokines, with proinflammatory activity [6]. Similarly to visceral fat, EF may promote the progression of atherosclerosis and it is associated with acute and chronic cardiovascular events [4,9]. According to literature, the volume of EF is larger in overweight patients and in these patients it is characterized by lower attenuation values (i.e. more negative in terms of HU) [8]. Therefore, we obtained a map of quartile density distribution, but we cannot find any significant variation in terms of attenuation values between groups. The Agatston coronary calcium score was higher in overweight population, although not significant [14]. TSF was thicker in overweight patients, while the attenuation value presented no difference between groups.

Given the limitations of attenuation variations in terms of HU, we proposed a radiomic quantitative approach from images using a free available computer application [15]. Among the 294 radiomics features examined in our study we found some discriminating parameters showing that the texture analysis software can discover different characteristics of EF and TSF if compared to a conventional quantification software (Figs. 4 and 5). In particular, EF showed in the two groups different distribution of attenuation values especially within the 50th percentile, with discriminating first-order radiomics features of the histogram class (i.e. mean, 0,1st, 10th, and 50th percentiles), and presented higher heterogeneity of grey-levels in extreme values deviating from the mean, with a discriminating second-order radiomic feature of co-occurrence matrix class (DifVarnc). We also checked for regional differences of EF and found some discriminating parameters depending on BMI at certain landmarks (i.e. in the right atrio-ventricular groove and in the anterior interventricular groove) with a potential correlation between grey-level values of matrix depending on the anatomical

Table 1
Patients characteristics.

Characteristics	Group A	Group B	p
Familiarity, n (%)	13 (43%)	13 (43%)	1
Smoke, n (%)	15 (50%)	18 (60%)	0.43
Diabetes, n (%)	3 (10%)	6 (20%)	0.57
Hypertension, n (%)	14 (46%)	18 (60%)	0.43
Hypercholesterolemia, n (%)	14 (46%)	19 (63%)	0.29
Mean age, years	60.6	63.3	0.07
Male/female, n	20/10	20/10	1
Agatston calcium score	97 $\pm$ 167	468 $\pm$ 1410	0.15

Table 2
Epicardial fat and subcutaneous thoracic fat characteristics detected with a dedicated software.

Characteristics	Group A mean ± SD	Group B mean ± SD	p
Epicardial fat volume (cm3)	86.3 ± 41.8	116.1 ± 49	0.014
Q1 (%)	3.7 ± 1.4	3.8 ± 1.9	0.83
Q2 (%)	15.9 ± 4.8	17.2 ± 3.9	0.22
Q3 (%)	39.8 ± 4.7	40 ± 3.2	0.83
Q4 (%)	40.7 ± 7.9	38.7 ± 5.5	0.34
Epicardial fat attenuation (HU)	−68 ± 5	−69.5 ± 4.9	0.28
Subcutaneous thoracic fat attenuation (HU)	−97.3 ± 19	−95.8 ± 19	0.75
Subcutaneous thoracic fat thickness (mm)	15 ± 6.2	19.5 ± 5.3	0.003

Table 3
Main radiomic features of epicardial fat between populations.

Radiomic features	Average values of group A	Average values of group B	p	Population with higher average values
Mean	54927	29900	0.02	A
Perc. 01%	3.766	1.355	0.001	A
Perc. 10%	4.322	1.722	0.002	A
Perc. 50%	6.844	4.366	0.02	A
S(2,2)DifVarnc	882	4270	0.007	B
Skewness	5985240	8702155	0.25	B
Kurtosis	4741204	4271721	0.96	A
S(1,-1)Entropy	260984	620525	0.09	B
S(1,-1) Contrast	0.02	0.25	0.058	B

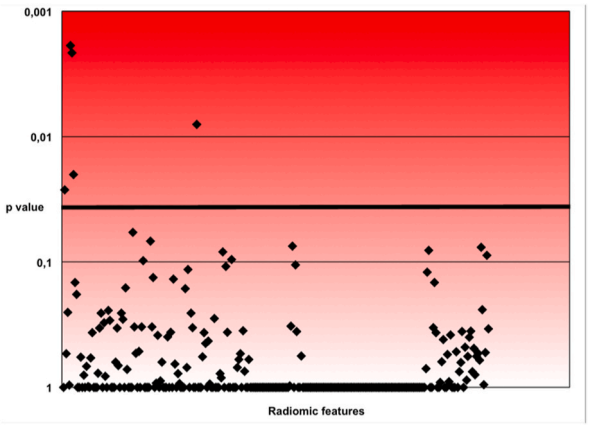

Fig. 4. Plot describing the p values of radiomic features in epicardial fat with bar of significance set at $p < 0.05$.

position. EF could have different metabolic characteristics depending on the anatomical position and coronary artery location [16].

Texture analysis of TSF showed that patients with BMI ≤25 kg/m^2 have different radiomic features compared to patients with BMI >25 kg/m^2, similarly to EF. TSF of group A showed specific attenuation values distribution, with discriminating parameters of the histogram class (10th, 50th, and 90th percentiles), and co-occurrence matrix characteristics, with discriminating parameters such as S (0,1)SumAverg, S(1,-1)SumOfSqs, S(3,0)Contrast, S(3,0)SumAverg, and S(4,0)SumAverg.

With reference to the grey-level run-length matrix TSF of group A had a rather not-uniform and disarranged texture (higher Horzl_RLNonUni), while TSF of group B presented a coarser structural texture (higher Vertl_LngREmph). In this regard, the composition of TSF varies as the BMI varies; the differences can be better discovered by texture analysis software.

Our study provided also some potential insights regarding different characteristics of EF and TSF [17]. The EF originates from splanchnopleuric mesoderm [18] and expresses uncoupling protein-1 (UCP-1, OMIM 113730) in their membranes suggesting that it could function similarly to the brown adipose tissue (i.e. heat production), despite being phenotypically similar to white adipose tissue [19,20]. TSF is a typical white adipose tissue deriving from mesodermal stem cells; it is considered responsible for fat storage and energy reservoir [21]. EF may protect the myocardium with transformation of white cells to the so called “beige” adipose cells in case of prolonged exposure to cold weather and β-adrenergic agonist [22], avoiding the development of ventricular arrhythmias [19]. Nonetheless, EF is associated with coronary events [23], BMI, obesity [24] and metabolic syndrome [25], with changes after statins administration [26]. Density characteristics can be assessed with CT and may provide the theoretical substrate of adipose cells transition and biological changes of EF like brown-white fat transformation and fibrosis, as opposed to mere quantification of volume

Table 4
Significant features between different ROIs landmarks calculated with Anova test in group A and in group B.

GROUP A S(2,0)Correlat (p = 0.04)			
ROIs	Mean	SD	Standard error
Red	−0.1975	0.2245	0.041
Green	−0.0678	0.3837	0.07
Blue	0.0202	0.3768	0.0688
GROUP A S(3,0)Correlat (p = 0.04)			
ROIs	Mean	SD	Standard error
Red	−0.4219	0.4266	0.0779
Green	−0.3012	0.374	0.0683
Blue	−0.1699	0.3296	0.0602
GROUP A S(4,0)Correlat (p = 0.03)			
ROIs	Mean	SD	Standard error
Red	−0.5254	0.4217	0.077
Green	−0.3057	0.4672	0.0853
Blue	−0.2048	0.5551	0.1013
GROUP B S(0,3)Correlat (p = 0.04)			
ROIs	Mean	SD	Standard error
Red	−0.2535	0.516	0.0942
Green	−0.3717	0.351	0.0641
Blue	−0.0807	0.4702	0.0858

Table 5
Radiomic features of thoracic subcutaneous fat tissue.

Radiomic features	Group A	Group B	p	Population with higher average values
Perc.10%	3.633	1	0.03	A
Perc.50%	5.566	1.7	0.01	A
Perc.90%	10	6.233	0.04	A
S(0,1)SumAverg	31590909	19545455	0.02	A
S(1,-1)SumOfSqs	2339	0	0.02	A
S(3,0)Contrast	0.1	0	0.03	A
S(3,0)SumAverg	1.533	1.166	0.02	A
S(4,0)SumAverg	3.1	1.733	0.04	A
Horzl_RLNonUni	20344290	7835979	0.02	A
Vertl_LngREmph	9505920	29831169	0.0005	B

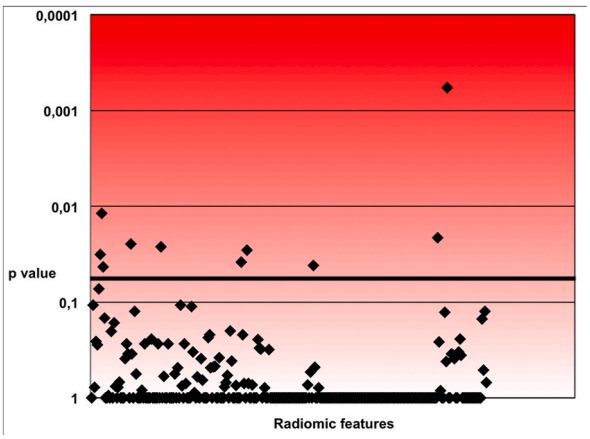

Fig. 5. Plot describing the p values of radiomic features in thoracic subcutaneous fat with bar of significance set at $p < 0.05$.

[27,28]. In this regard a radiomic texture analysis of EF density may provide a better understanding of this undiscovered phenomenon.

However, there are some aspects that do not allow easy use of radiomics in this field because of poor reproducibility and lack of standardization with different CT protocols and scanners [29]. The radiomic features show the spatial distribution of numerical values corresponding to grey values in the images for a defined tissue [30]. The texture analysis is the result of some steps: image acquisition,

image segmentation (manual, semiautomatic or automatic), and features extraction [31].

Texture analysis could be used not only in oncology but also in cardiovascular radiology to study the EF or TSF [32]. Recent data showed that patients with acute myocardial infarction have a distinct EF radiomic phenotype compared with patients with stable or no coronary artery disease [33]. The lack of standardization of image acquisition including patient position, pixel size, slice thickness, reconstruction algorithms has led to great variability of radiomic features [34]. This makes it difficult to standardize the results obtained with different CT equipments especially in absence of a reproducible segmentation technique [35]. In this regard our data cannot be generalised to other equipments. This study is also limited by its retrospective nature and by the small number of patients of the two populations. It could be interesting to monitor the features of EF and TSF over time with correlation to major cardiac events [6, 29].

5. Conclusions

Texture analysis provides detailed evaluation of EF and TSF. EF and TSF had different radiomic features as the BMI varies. Radiomics may provide relevant information over EF and TSF texture analysis for cardiovascular risk prediction beyond conventional images. Reproducibility and standardization of radiomics application are mandatory to support the clinical use in this field.

Author contribution statement

Manfredi Agnese, M.D.; Patrizia Toia, M.D.; Giulia Sollami, M.D.; Carmelo Militello; Leonardo Rundo; Salvatore Vitabile; Erica Maffei, M.D.; Francesco Agnello, M.D.; Cesare Gagliardo, M.D.; Emanuele Grassedonio, M.D.; Massimo Galia, M.D.; Filippo Cademartiri; Massimo Midiri, M.D.; Ludovico La Grutta, M.D.: Conceived and designed the experiments; Performed the experiments; Analyzed and interpreted the data; Contributed reagents, materials, analysis tools or data; Wrote the paper.

Data availability statement

The data that has been used is confidential, including data of dedicated computer applications at the local institution. However, data may be available on a reasonable individual request upon approval of all authors.

Declaration of competing interest

The authors declare that they have no known competing financial interests or personal relationships that could have appeared to influence the work reported in this paper.

References

[1] B. Gaborit, C. Sengenes, P. Ancel, A. Jacquier, A. Dutour, Role of epicardial adipose tissue in health and disease: A Matter of Fat? Comp. Physiol. 7 (2017) 1051–1082, https://doi.org/10.1002/cphy.c160034.
[2] G. Iacobellis, F. Assael, M.C. Ribaudo, et al., Epicardial fat from echocardiography: a new method for visceral adipose tissue prediction, Obes. Res. 11 (2003) 304–310, https://doi.org/10.1038/oby.2003.45.
[3] H.S. Sacks, J.N. Fain, Human epicardial adipose tissue: a review, Am. Heart J. 153 (2007) 907–917, https://doi.org/10.1016/j.ahj.2007.03.019.
[4] A. Hiuge-Shimizu, K. Kishida, T. Funahashi, et al., Coexistence of visceral fat and multiple risk factor accumulations is strongly associated with coronary artery disease in Japanese (the VACATION-J study), J. Atherosclerosis Thromb. 19 (2012) 657–663, https://doi.org/10.5551/jat.13037.
[5] G.H. Goossens, The metabolic phenotype in obesity: fat mass, body fat distribution, and adipose tissue function, Obes. Facts 10 (2017) 207–215, https://doi.org/10.1159/000471488.
[6] M. Goeller, S. Achenbach, M. Marwan, et al., Epicardial adipose tissue density and volume are related to subclinical atherosclerosis, inflammation and major adverse cardiac events in asymptomatic subjects, J. Cardiovas. Comp. Tomog. 12 (2018) 67–73, https://doi.org/10.1016/j.jcct.2017.11.007.
[7] S.W. Rabkin, Epicardial fat: properties, function and relationship to obesity, Obes. Rev. 8 (2007) 252–261, https://doi.org/10.1111/j.1467-789X.2006.00293.x.
[8] G. Milanese, M. Silva, L. Bruno, et al., Quantification of epicardial fat with cardiac CT angiography and association with cardiovascular risk factors in symptomatic patients: from the ALTER-BIO (Alternative Cardiovascular Bio-Imaging markers) registry, Diagn. Interv. Radiol. 25 (2019) 35–41, https://doi.org/10.5152/dir.2018.18037.
[9] G. Iacobellis, F. Leonetti, N. Singh, M. Sharma, Relationship of epicardial adipose tissue with atrial dimensions and diastolic function in morbidly obese subjects, Int. J. Cardiol. 115 (2007) 272–273, https://doi.org/10.1016/j.ijcard.2006.04.016.
[10] L. La Grutta, P. Toia, A. Farruggia, et al., Quantification of epicardial adipose tissue in coronary calcium score and CT coronary angiography image data sets: comparison of attenuation values, thickness and volumes, Br. J. Radiol. 89 (1062) (2016), 20150773, https://doi.org/10.1259/bjr.20150773.
[11] C. Militello, L. Rundo, P. Toia, et al., A semi-automatic approach for epicardial adipose tissue segmentation and quantification on cardiac CT scans, Comput. Biol. Med. 114 (2019), 103424, https://doi.org/10.1016/j.compbiomed.2019.103424.
[12] A.S. Agatston, W.R. Janowitz, F.J. Hildner, N.R. Zusmer, M. Viamonte Jr., R. Detrano, Quantification of coronary artery calcium using ultrafast computed tomography, J. Am. Coll. Cardiol. 15 (1990) 827–832, https://doi.org/10.1016/0735-1097(90)90282-t.
[13] P.M. Szczypiński, M. Strzelecki, A. Materka, A. Klepaczko, et al., MaZda-a software package for image texture analysis, Comput. Methods Progr. Biomed. 94 (2009) 66–76, https://doi.org/10.1016/j.cmpb.2008.08.005.
[14] B.T. Franssens, H.M. Nathoe, F.L.J. Visseren, Y. der Graaf, T. Leiner, SMART Study Group, Relation of epicardial adipose tissue radiodensity to coronary artery calcium on cardiac computed tomography in patients at high risk for cardiovascular disease, Am. J. Cardiol. 119 (2017) 1359–1365, https://doi.org/10.1016/j.amjcard.2017.01.031.
[15] P. Lambin, E. Rios-Velazquez, R. Leijenaar, et al., Radiomics: extracting more information from medical images using advanced feature analysis, Eur. J. Cancer 48 (2012) 441–446, https://doi.org/10.1016/j.ejca.2011.11.036.
[16] Z. Liu, S. Wang, Y. Wang, et al., Association of epicardial adipose tissue attenuation with coronary atherosclerosis in patients with a high risk of coronary artery disease, Atherosclerosis 284 (2019) 230–236, https://doi.org/10.1016/j.atherosclerosis.2019.01.033.
[17] A. Vargas-Castillo, R. Fuentes-Romero, L.A. Rodriguez-Lopez, N. Torres, A.R. Tovar, Understanding the biology of thermogenic fat: is browning A new approach to the treatment of obesity? Arch. Med. Res. 48 (2017) 401–413, https://doi.org/10.1016/j.arcmed.2017.10.002.

[18] Y.Y. Chau, R. Bandiera, A. Serrels, et al., Visceral and subcutaneous fat have different origins and evidence supports a mesothelial source, Nat. Cell Biol. 16 (2014) 367–375, https://doi.org/10.1038/ncb2922.
[19] H.S. Sacks, J.N. Fain, B. Holman, et al., Uncoupling protein-1 and related messenger ribonucleic acids in human epicardial and other adipose tissues: epicardial fat functioning as brown fat, J. Clin. Endocrinol. Metab. 94 (2009) 3611–3615, https://doi.org/10.1210/jc.2009-0571.
[20] T.P. Fitzgibbons, M.P. Czech, Epicardial and perivascular adipose tissues and their influence on cardiovascular disease: basic mechanisms and clinical associations, J. Am. Heart Assoc. 3 (2) (2014), e000582, https://doi.org/10.1161/JAHA.113.000582.
[21] M.T. Hyvönen, K.L. Spalding, Maintenance of white adipose tissue in man, Int. J. Biochem. Cell Biol. 56 (2014) 123–132, https://doi.org/10.1016/j.biocel.2014.09.013.
[22] N. Lanthier, I.A. Leclercq, Adipose tissues as endocrine target organs, Best Pract. Res. Clin. Gastroenterol. 28 (2014) 545–558, https://doi.org/10.1016/j.bpg.2014.07.002.
[23] A.A. Mahabadi, M.H. Berg, N. Lehmann, et al., Association of epicardial fat with cardiovascular risk factors and incident myocardial infarction in the general population: the Heinz Nixdorf Recall Study, J. Am. Coll. Cardiol. 61 (2013) 1388–1395, https://doi.org/10.1016/j.jacc.2012.11.062.
[24] M.A. Exley, L. Hand, D. O'Shea, L. Lynch, Interplay between the immune system and adipose tissue in obesity, J. Endocrinol. 223 (2014) R41–R48, https://doi.org/10.1530/JOE-13-0516.
[25] H. Yorgun, U. Canpolat, T. Hazırolan, et al., Increased epicardial fat tissue is a marker of metabolic syndrome in adult patients, Int. J. Cardiol. 165 (2013) 308–313, https://doi.org/10.1016/j.ijcard.2011.08.067.
[26] J.H. Park, Y.S. Park, Y.J. Kim, et al., Effects of statins on the epicardial fat thickness in patients with coronary artery stenosis underwent percutaneous coronary intervention: comparison of atorvastatin with simvastatin/ezetimibe, J. Cardiovas. Ultrasound 18 (2010) 121–126, https://doi.org/10.4250/jcu.2010.18.4.121.
[27] A. Gifford, T.F. Towse, R.C. Walker, M.J. Avison, E.B. Welch, Characterizing active and inactive brown adipose tissue in adult humans using PET-CT and MR imaging, Am. J. Physiol. Endocrinol. Metab. 311 (2016) E95–E104, https://doi.org/10.1152/ajpendo.00482.2015.
[28] N.N. Pandey, S. Sharma, P. Jagia, S. Kumar, Epicardial fat attenuation, not volume, predicts obstructive coronary artery disease and high risk plaque features in patients with atypical chest pain, Br. J. Radiol. 93 (1114) (2020), 20200540, https://doi.org/10.1259/bjr.20200540.
[29] C. Militello, F. Prinzi, G. Sollami, L. Rundo, L. La Grutta, S. Vitabile, CT radiomic features and clinical biomarkers for predicting coronary artery disease, Cogn. Comp. (2023), https://doi.org/10.1007/s12559-023-10118-7.
[30] W.A. Kalender, CT: the unexpected evolution of an imaging modality, Eur. Radiol. 15 (Suppl 4) (2005) D21–D24, https://doi.org/10.1007/s10406-005-0128-3.
[31] S.J. Ahn, J.H. Kim, S.M. Lee, S.J. Park, J.K. Han, CT reconstruction algorithms affect histogram and texture analysis: evidence for liver parenchyma, focal solid liver lesions, and renal cysts, Eur. Radiol. 29 (2019) 4008–4015, https://doi.org/10.1007/s00330-018-5829-9.
[32] M. van Assen, G. Muscogiuri, D. Caruso, et al., Artificial intelligence in cardiac radiology, Radiol. Med. 125 (2020) 1186–1199, https://doi.org/10.1007/s11547-020-01277-w.
[33] A. Lin, M. Kolossváry, J. Yuvaraj, et al., Myocardial infarction associates with a distinct pericoronary adipose tissue radiomic phenotype: a prospective case-control study, JACC Cardiovasc. Imag. 13 (2020) 2371–2383, https://doi.org/10.1016/j.jcmg.2020.06.033.
[34] S.S. Yip, H.J. Aerts, Applications and limitations of radiomics, Phys. Med. Biol. 61 (2016) R150–R166, https://doi.org/10.1088/0031-9155/61/13/R150.
[35] P. Lambin, R.T.H. Leijenaar, T.M. Deist, et al., Radiomics: the bridge between medical imaging and personalized medicine, Nat. Rev. Clin. Oncol. 14 (2017) 749–762, https://doi.org/10.1038/nrclinonc.2017.141.